Deep-Sea Research II ▮ (▮▮▮▮) ▮▮▮–▮▮▮

Contents lists available at SciVerse ScienceDirect

Deep-Sea Research II

journal homepage: www.elsevier.com/locate/dsr2

Changes in partitioning of carbon amongst photosynthetic pico- and nano-plankton groups in the Sargasso Sea in response to changes in the North Atlantic Oscillation

John R. Casey [a,b], Jerome P. Aucan [a,c], Stacey R. Goldberg [a], Michael W. Lomas [a,*,1]

[a] Bermuda Institute of Ocean Sciences, 17 Biological Lane, Ferry Reach, St. Georges, GE-01, Bermuda
[b] School of Ocean and Earth Science and Technology, University of Hawaii, Manoa, 1000 Pope Rd., Honolulu, HI 96822, USA
[c] Institut de Recherche pour le Développement, Laboratoire d'Etudes en Géophysique et Océanographie Spatiale, 14 Av. Edouard Belin, 31400 Toulouse, France

ARTICLE INFO

Keywords:
Bermuda Atlantic Time-series Study
Phytoplankton biomass
Cyanobacteria
Picoeukaryotes
North Atlantic Oscillation
Cellular carbon content

ABSTRACT

Picophytoplankton carbon biomass at the Bermuda Atlantic Time-series Study (BATS) site from June 2004 to December 2010 was estimated from the direct calibration of cellular carbon content and forward light scatter (via flow cytometry). Seasonality and interannual dynamics of *Prochlorococcus*, *Synechococcus* and small eukaryotic algae (<12 μm diameter) abundance, cellular carbon content (Q_C; particulate organic carbon; POC cell^{-1}), and group-specific carbon biomass are reported. Q_C of individual taxa varied with depth and season by as much as an order of magnitude, roughly comparable to variability in abundance. During the time-series there were obvious shifts in the taxonomic distribution of photosynthetic carbon biomass; these interannual shifts in biomass were due to simultaneous changes in both Q_C and cell abundance. The observed pattern was not apparent from numerical abundance alone, highlighting the importance of Q_C measurements in place of using fixed conversion factors to better understand biological carbon dynamics. Changes in the phase of the North Atlantic Oscillation (NAO) from positive to negative modes correlated with shifts in biomass between picocyanobacteria and small eukaryotic algae, respectively. Thus, shifts in algal community structure are inferred to be associated with changes in light intensity and implied nutrient supply via mixing (*i.e.*, patterns in upper ocean stability). These observed changes in phytoplankton biomass partitioning were correlated with the important ocean carbon cycle parameters of export flux, mesopelagic transfer efficiency, and elemental stoichiometry. Importantly, interannual relationships between these parameters and algal biomass were detected only when Q_C was considered as variable.

1. Introduction

Robust taxonomically resolved estimates of living biomass are vital to understand the turnover and flux of particulate organic carbon (POC) in the global ocean (Huot et al., 2007; Buitenhuis et al., in press). To date, few studies have specifically addressed or directly estimated living autotrophic carbon in marine systems (Karl and Bossard, 1985; Robertson et al., 1998; DuRand et al., 2001; Grob et al., 2007), partly because of difficulties in separating microbes from detritus with overlapping size spectra. Instead, biomass is often estimated assuming a static scalar conversion from abundance to biomass for a particular taxonomic group. Nevertheless, cellular carbon content (Q_C) is expected to vary systematically across all levels of biological diversity and cell physiology according to cell cycle stage, nutritional status, and to accommodate changes in pigment content (Chisholm, 1992; Marañón et al., 2007; Marañón, 2008; Key et al., 2010). Although group-specific responses to environmental perturbations vary, some generalizations may be useful for interpretation of changes in Q_C. The most striking adjustments to Q_C are associated with changes in light intensity during stratified periods. Additionally, annual winter mixing exposes chronically nutrient stressed surface algae to elevated nutrient concentrations and decreased light intensity with combined physiological effects lending to higher Q_C (*e.g.*, Chisholm, 1992; Chen et al., 2010). Because environmental perturbations may influence physiological attributes on time scales shorter than changes in population size (*e.g.*, Fawcett and Ward, 2011), and physiological responses may be uncoupled from biomass responses (*e.g.*, tight grazer control on picoplankton) variations in Q_C may reveal spatial and temporal heterogeneity that estimates of biomass scaled from abundance alone may mask. Similarly, interannual shifts in community composition associated with large-scale physical forcing are likely to be accompanied by

* Corresponding author. Tel.: +1 202 747 3255x311; fax: +1 202 747 3257.
E-mail address: mlomas@bigelow.org (M.W. Lomas).
[1] Present address: Bigelow Laboratory for Ocean Sciences, 60 Bigelow Drive, East Boothbay, ME 04543, USA.

0967-0645/$ - see front matter © 2013 Elsevier Ltd. All rights reserved.
http://dx.doi.org/10.1016/j.dsr2.2013.02.002

physiological responses to variability in nutrient supply and hydrographic conditions, which may not necessarily translate into changes in cell abundance alone.

The most common metrics used to estimate taxonomically resolved autotrophic POC are acquired from cultured isolates (Table 1). Despite expansive biogeography and high numerical abundance, few cultured strains are available as representatives of the dominant oligotrophic phytoplankton taxa (*e.g. Prochlorococcus*, *Synechococcus*, Pelagophyceae, Prymnesiophyceae, Bacillariophyceae, Chlorophyceae); fewer still are axenic. Furthermore, laboratory isolates are typically poor physiological representatives of the natural assemblage, due in part to limited representation of the total diversity and due to difficulties in reproducing environmental conditions and variability in the laboratory. The carbon content of individual cells or populations is otherwise estimated by chlorophyll to carbon or volume to carbon relationships, with volume estimated by optical backscattering, beam attenuation, microscopy sizing, impedance, or measured with ion beam sputtering (*e.g.* nanoSIMS; references in Table 1). These methods vary considerably in both throughput and precision.

A 6.5-year time-series record of cyanobacterial and eukaryotic algal abundance, Q_C and group-specific biomass, based on an

Table 1
Collection of Q_C from relevant literature. Q_C data from this study were reported for each algal group in three criteria: (1) "Stratified period euphotic zone"- mean Q_C from 0–120 m from April to November; (2) "Mixed period"- mean Q_C from 0–250 m from December to March; (3) "Stratified period sub-euphotic zone"- mean Q_C from 120–250 m from April to November. Q_C values are reported as range or mean ± standard deviation (sd), where appropriate. FSC—forward scatter; P—phosphorus; POC—particulate organic carbon; TEM—transmission electron microscopy; P–I—photosynthesis versus irradiance; P_i^{cell}—cell-specific photosynthetic performance [fg C cell^{-1} h^{-1}]; μ—specific growth rate [h^{-1}]; HL—high light adapted; LL—low light adapted; PE— phycoerythrin (pigment);

Algal group	Q_C [fg C cell^{-1}]	Method	Conversion factor	Reference
Prochlorococcus				
	52 ± 19	FSC pulse height: Stratified period euphotic zone	none	This study
	78 ± 19	FSC pulse height: Mixed period	none	This study
	158 ± 27	FSC pulse height: Stratified period sub-euphotic zone	none	This study
	46 to 61	Particulate carbon, P-replete or P-limited axenic strain MED4	none	Bertilsson et al. (2003)
	61	Chlorophyll to carbon	55 g C (gChl a)$^{-1}$	Blanchot and Rodier (1996)
	49 ± 9	POC non-axenic cultures, corrected for contaminating bacteria	none	Cailliau et al. (1996)
	53	Volume to carbon, assuming 0.6 μm diameter	470 fg C μm^{-3}	Campbell et al. (1994)
	17 to 38	POC, axenic culture (high irradiance)	none	Claustre et al. (2002)
	54	Volume to carbon (discrete size measurements from FCM)	325 fg C μm^{-3}	Durand et al. 2001
	32 to 72	Volume to carbon, flow cytometry sizing	235 fg C μm^{-3}	Garrison et al. (2000)
	29 ± 11	Volume to carbon, beam attenuation, sorting, impedance	none	Grob et al. (2007)
	6 to 90	TEM X-ray microanalysis of several strains	none	Heldal et al. (2003)
	30	Volume to carbon, microscopy, "Very small red fluorescing cells"	220 fg C μm^{-3}	Ishizaka et al. (1994)
	100	Volume to carbon, flow cytometry sizing	190 fg C μm^{-3}	Landry and Kirchman (2002)
	53 to 59	Volume to carbon, assuming 0.8 μm diameter	220 fg C μm^{-3}	Li et al. (1992)
	61 to 94	Based on P-I estimates for 6 HL isolates	$(P_i^{cell} \times 14)/\mu$	Moore (1997)
	250 ± 56	Based on P-I estimates for 2 LL isolates	$(P_i^{cell} \times 14)/\mu$	Moore (1997)
	15 to 152	Volume to carbon, Coulter and flow cytometry sizing	235 fg C μm^{-3}	Shalapyonok et al. (2001)
	78	Dry weight, based on strain MED4	50% of DW	Shaw (2001)
	92	Consumption of added nitrogen in batch culture	C:N ratio of 6	Veldhuis et al. (1997)
	35	Volume to carbon, size fractionation; PE negative cells	220 fg C μm^{-3}	Veldhuis and Kraay (2004)
	50	Volume to carbon, size fractionation; PE positive cells	220 fg C μm^{-3}	Veldhuis and Kraay (2004)
	29	Volume to carbon, size fractionation	200 fg C μm^{-3}	Zubkov et al. (2000)
	38 to 42	Volume to carbon, Coulter and flow cytometry sizing	240 fg C μm^{-3}	Worden et al. (2004)
Synechococcus				
	250 ± 91	FSC pulse height: Stratified period euphotic zone	none	This study
	305 ± 47	FSC pulse height: Mixed period	none	This study
	434 ± 141	FSC pulse height: Stratified period sub-euphotic zone	none	This study
	92 to 244	Particulate carbon, P-replete or P-limited axenic strain MED4	none	Bertilsson et al. (2003)
	104	Chlorophyll to carbon, volume ratio of *Syn:Pro*	Syn $C = 1.7 \times$ Pro C	Blanchot and Rodier (1996)
	112	Volume to carbon (discrete size measurements from FCM)	325 fg C μm^{-3}	Durand et al. 2001
	250	Volume to carbon, microscopy	250 fg C μm^{-3}	Fuhrman et al. (1989)
	101 to 152	Volume to carbon, flow cytometry sizing	235 fg C μm^{-3}	Garrison et al. (2000)
	60 ± 19	Volume to carbon, beam attenuation, sorting, impedance	none	Grob et al. (2007)
	40 to 550	TEM X-ray microanalysis, 2 strains, various growth media	none	Heldal et al. (2003)
	83	Volume to carbon, microscopy sizing	220 fg C μm^{-3}	Ishizaka et al. (1994)
	250	Particulate carbon	none	Kana and Glibert (1987)
	100	Volume to carbon, flow cytometry sizing	190 fg C μm^{-3}	Landry and Kirchman (2002)
	49 to 274	Volume to carbon, Coulter and flow cytometry sizing	235 fg C μm^{-3}	Shalapyonok et al. (2001)
	175	Nutrient consumption in culture	C:N ratio of 6	Veldhuis et al. (1997)
	59 to 78	Volume to carbon, Coulter and flow cytometry sizing	230 fg C μm^{-3}	Worden et al. (2004)
Picoeukaryotes				
	2587 ± 554	FSC pulse height: Stratified period euphotic zone	none	This study
	2301 ± 735	FSC pulse height: Mixed period	none	This study
	2732 ± 661	FSC pulse height: Stratified period sub-euphotic zone	none	This study
	3110	Volume to carbon, assuming 3.0 μm diameter	220 fg C μm^{-3}	Blanchot and Rodier (1996)
	3980 ± 732	Volume to carbon, microscopy	220 fg C μm^{-3}	Fuhrman et al. (1989)
	1011	Volume to carbon, assuming 1.5 μm diameter	$0.94(\log V) - 0.60$	Garrison et al. (2000)
	730 ± 226	Volume to carbon, beam attenuation, sorting, impedance	none	Grob et al. (2007)
	436	Volume to carbon, microscopy, red fluorescing	220 fg C μm^{-3}	Ishizaka et al. (1994)
	1836	Volume to carbon, microscopy, orange fluorescing	220 fg C μm^{-3}	Ishizaka et al. (1994)
	1800 to 3000	Volume to carbon, size fractionation	220 fg C μm^{-3}	Veldhuis et al. (1997)
	162 to 488	Volume to carbon, Coulter and flow cytometry sizing	238 fg C μm^{-3}	Worden et al. (2004)

Please cite this article as: Casey, J.R., et al., Changes in partitioning of carbon amongst photosynthetic pico- and nano-plankton groups in the Sargasso Sea in.... Deep-Sea Res. II (2013), http://dx.doi.org/10.1016/j.dsr2.2013.02.002

empirical calibration between forward angle light scatter (FSC) and Q_C, is presented for the northwestern Sargasso Sea at the BATS site. It is hypothesized that changes in the North Atlantic Oscillation (NAO) phase shifts the autotrophic community structure between assemblages dominated by picocyanobacteria and eukaryotic algae. This change in community structure is manifested not only in changes in relative cell abundance but in changes in Q_C as well. Findings from this study suggest that quantification of Q_C will bolster the link between regional climate and net phytoplankton biomass responses, and should improve our understanding of the relationships between cell size and mechanisms of carbon export (*e.g.*, Lomas and Moran, 2010) and skill of coupled ocean ecosystem-biogeochemical models (*e.g.*, Dunne et al., 2010)

2. Methods

2.1. Site description

The Bermuda Atlantic Time-series Study (BATS) site is positioned in the western Sargasso Sea between the permanently stratified North Atlantic Equatorial Current and subtropical convergence zone (SCZ; ca. 25°N to 32°N; Halliwell and Cornillon, 1990a,b; Hanson et al., 1991) to the south and the North Atlantic 18 °C mode water formation region to the immediate north (Worthington, 1976; Talley and Raymer, 1982; Woods and Barkman, 1986). The BATS site, situated at 31°40′N 64°10′W, lies in a hydrographic and biogeochemical transition region (*e.g.*, Siegel et al., 1990; Curry et al., 1998). Spatially, algal community structure in the western Sargasso Sea exhibits a strong meridional diversity procession from diatom, chlorophyte and prymnesiophyte dominated biomass north of ~33°N to a *Prochlorococcus* (and cyanobacteria in general) dominated SCZ south of ~30°N (Zwirglmaier et al., 2007; Follows and Dutkiewicz, 2011). Ventilation of 18 °C mode water and subsequent phytoplankton community response in the 30–33°N transition zone are postulated to be highly sensitive to changes in regional weather patterns (Siegel et al., 1990). Thus, this is an ideal location to separate biomass responses expressed in terms of variable Q_C from numerical abundance responses to physical perturbations that alter nutrient supply and light availability.

2.2. Calibration of cellular POC and forward scatter

An empirical calibration was performed between the geometric mean forward scatter pulse height (FSC-H) of a population and average cellular Q_C from those same cells sorted and measured on an elemental analyzer for POC. Both cultured isolates and natural populations of algae in the pico- and nano-size range (approximately 0.2–12 μm) were included in the calibration.

2.2.1. Cultured cells

A variety of cell cultures were used to calibrate Q_C to FSC-H. Cell cultures of *Prochlorococcus marinus*, *Synechococcus* sp., *Emiliania huxleyi*, *Scrippsiella* sp., and *Thalassiosira oceanica* were acquired from the Provasoli-Guillard National Center for Marine Algae and Microbiota (formerly Provasoli-Guillard Center for Culture of Marine Phytoplankton (CCMP), http://www.ncma.bigelow.org) and transferred aseptically to appropriate media (Guillard, 1983). *Prochlorococcus* was incubated with Pro99 media (Moore et al., 2007), *Synechococcus* in F/2-Si, *E. huxleyi*, *Scrippsiella* sp. and *T. oceanica* in F/2. All culture media was made using autoclave sterilized filtered (0.22 μm) low nutrient Sargasso seawater and filter sterilized media amendments. Cells were maintained at 21 °C on an 18:6 h light:dark cycle at ~100 μmol photons m^{-2} s^{-1}. Triplicate tubes were shaded to roughly 100%, 50%, 10%, and 1% of ambient irradiance to change chlorophyll per cell and thus a range of carbon $cell^{-1}$ values for *Prochlorococcus marinus*, *Synechococcus* sp., and *T. oceanica*. Cell growth was monitored daily by in vivo fluorescence with a Turner TD-700 fluorometer and harvested during lag, exponential, and stationary phase growth for flow cytometry sorting and elemental analysis as detailed below. Paired samples from a subset of these cultures were collected with one sample fixed with paraformaldehyde (0.5% *v*/*v*), inverted and incubated in the dark at 4 °C for ~1 h and the other kept live to correct for the effect of fixation on refractive index. Live and fixed samples were processed immediately.

2.2.2. Natural populations

In addition to cultured populations, natural populations were also collected to augment the FSC-Q_C calibration. Samples for Q_C measurements in natural populations were collected from the BATS site during the spring of 2010 from near-surface, 40 m, and the deep chlorophyll maximum (DCM; 80 m) in 20L carboys and refrigerated in the dark for one day until further processing on shore. Cells were gently (< 15 mm Hg vacuum) concentrated onto 47 mm 0.4 μm polycarbonate membrane filters (Millipore Inc., Bellerica, MA). Filters were transferred with a small remaining volume to 5 ml polyethylene cryovials and refrigerated until flow cytometry sorting as below. To relate the calibration curve to fixed natural populations, duplicate tubes were fixed with paraformaldehyde (0.5% v/v), inverted and incubated in the dark at 4 °C for ~1 h according to standard BATS flow cytometry sample preparation procedures (Casey et al., 2007). Live and fixed samples were processed within 48 h of collection. A second experiment with live and fixed natural samples from Ferry Reach (nearby the Bermuda Institute of Ocean Sciences; BIOS) were treated identically and processed immediately to identify potential sample storage effects.

2.2.3. Sample preparation for flow cytometric sorting and analysis

Cultured isolates and natural samples were gently agitated to remove as many cells as possible from the tube walls and the filter. Frozen fixed samples were thawed in the dark at 4 °C. Cells in solution were filtered through a 35 μm Nitex mesh in order to remove the occasional large particle and any cell aggregates that might clog the nozzle tip. If necessary, culture samples were diluted with 0.2 μm filtered seawater so as to attain an appropriate cell concentration for flow cytometric sorting (~20,000 total events s^{-1}). All samples were sorted at BIOS.

2.3. Environmental data

Flow cytometry samples for cell abundance were collected from June 2004 through December 2010 on monthly BATS cruises and biweekly during the spring bloom period (January through March). Samples were collected at 12 depths between 1–250 m (roughly 20 m intervals) in 2.0 mL polyethylene cryovials. Vials were rinsed 3 times with seawater sample, filled to 1.5 mL, fixed with paraformaldehyde (PFA; 0.5% final concentration) at 4 °C for ~1 h, flash frozen in liquid nitrogen, and stored at −80 °C until analysis.

Samples for POC were collected from the same depth intervals and processed according to standard BATS protocols (Steinberg et al., 2001). Samples for both bulk and sorted POC were dried at 60 °C overnight, fumed with concentrated hydrochloric (HCl) acid overnight, and dried again at 60 °C overnight before analysis on a Control Equipment 440 CHN elemental analyzer (Knap et al., 1997). Blank samples consisted of 2 ml of either 0.2 μm filtered

Please cite this article as: Casey, J.R., et al., Changes in partitioning of carbon amongst photosynthetic pico- and nano-plankton groups in the Sargasso Sea in.... Deep-Sea Res. II (2013), http://dx.doi.org/10.1016/j.dsr2.2013.02.002

seawater (bulk) or filtered sheath fluid (sorted) passed through an appropriate filter and analyzed as for the samples.

Photosynthetically active radiation (PAR) data were collected with a Satlantic Profiling Multi-channel Radiometer (Satlantic Inc., Halifax, Nova Scotia, Canada) at 4 Hz deployed to ~120 m at local noon following retrieval of the cast on which all other biological suite measurements were collected. Spectral downwelling irradiance (E_d) in the photosynthetically available wavelength range (E_{par}) was calculated as a derivation of Plank's Law for integrated E_d over the PAR range (400–700 nm) according to Siegel (1987).

Chlorophyll *a* was measured fluorometrically (Holm-Hansen and Riemann, 1978). Briefly, 500 ml samples were filtered onto GF/F filters, extracted in 90% acetone at −20 °C for >12 h, and read on a Turner 10AU fluorometer. The sample was then acidified with two drops of 1.2 M HCl and read again for phaeopigment correction. Fluorometric chlorophyll *a* data were not available for the period beginning October 2005 through August 2007. During this period HPLC chlorophyll *a* data were used (Van Heukelem and Thomas, 2001). Although replicate data were not available during this period by which to compare methods directly, fluorometric ($Chla_{fl}$) and HPLC chlorophyll *a* ($chla_{hplc}$) were in first-order agreement ($r^2=0.71$; $n=2625$; where $Chla_{fl}=0.87\times chla_{hplc}$) throughout the BATS record from November 1988 through September 2004. Differences between methods may introduce uncertainty so trends associated with chlorophyll *a* measurements are reported with and without these appended HPLC data (*e.g.*, Table 2). Temperature was recorded for each cast on a SeaBird SBE-911plus CTD, and discrete salinity samples were collected for analysis on a Guildline Autosol 8400A (Michaels and Knap, 1996). Mixed layer depth (MLD) was based on a change in sigma-t equivalent to a 0.2 °C decrease from the surface (Sprintall and Tomczak, 1992).

2.4. Particulate carbon and nitrogen flux

Export flux was collected by surface-tethered particle interceptor traps at 150, 200, and 300 m for 3 day deployments each cruise (Knauer et al., 1979). Baffled trap cylinders were filled with a brine solution (surface seawater amended with 50 g NaCl L^{-1}) and 0.7% *v*/*v* formaldehyde. Samples were concentrated onto 90 mm 0.8 μm polycarbonate membrane filters and dried to constant weight at 65 °C after removal of swimmers, fumed with HCl overnight, dried at 65 °C, and then analyzed for carbon and nitrogen content using a Control Equipment Model 440XA CHN elemental analyzer (Knap et al., 1997).

2.5. Flow cytometry analysis and cell sorting

2.5.1. Sort conditions

A high speed jet-in-air Influx™ Cell Sorter (formerly Cytopeia, Inc., Seattle, WA, now Becton Dickenson), modified for small particle detection with a 100X objective magnification, was used for all analysis and sorts. A 200 mW blue (488 nm) laser (Coherent Inc., Santa Clara, CA) run at full power, was used for excitation of autofluorescent cells. Analog pulse height signals from 580/30 nm (phycoerythrin; PE), 650 nm long-pass (Chl-a), 488 nm side scatter (SSC), and 488 nm forward scatter (FSC-H) channels were amplified with photomultiplier tubes (Hamamatsu Photonics K.K.) and log transformed. Triggering on FSC-H was used to ensure small (and dim) particle detection. Jet and optical alignments were optimized using 3.0 μm 8 peak UltraRainbow and 0.53 μm Nile Red polystyrene calibration particles (Spherotech Inc., Lake Forest, IL). A 70 μm ceramic nozzle tip was used at a sample pressure of 1.97 bar (+0.07 bar above sheath pressure) to optimize speed while maintaining high fluorescent yield, coherence of the core, particle focus, low turbulence at the core-jet interface, and ensuring laminar flow, all

Table 2
Influence of NAO phase on environmental and biological parameters. All values are averages (± standard deviation) over the winter period (Dec, Jan, Feb) for all NAO+ or NAO− years. Values in bold denote paired *t*-test significance ($P<0.05$). Areal concentrations were integrated from 0–250 m. SST—sea surface temperature; SSS—sea surface salinity; MLD—maximum mixed layer depth; POC—particulate organic carbon caught on a GF/F; Chl a—chlorophyll *a*; Autotrophic POC—measured as the sum of *Prochlorococcus*, *Synechococcus*, and eukaryotic algae POC; POC flux—C mass collected in surface tethered sediment traps deployed to 150, 200, and 300 m; T_{eff} —transfer efficiency measured as the percentage of C flux collected at different depth horizons (*i.e.*, 100 × POC flux at 300 m/POC flux at 200 m). *Average calculated without winter 2006 (HPLC method).

Variable	Taxon or depth	NAO+	NAO−
SST [°C]		20.55 ± 0.33	20.24 ± 0.20
SSS		36.68 ± 0.02	36.67 ± 0.09
MLD [max]		181 ± 45	**262 ± 94**
POC [g C m^{-2}]		4.78 ± 0.96	4.51 ± 0.86
Chl a [mg m^{-2}]		29 ± 12	34 ± 5 (32 ± 3)*
Autotrophic POC [g C m^{-2}]		1.81 ± 0.50	2.07 ± 1.02
Abundance [10^{12} cells m^{-2}]	*Prochlorococcus*	5.9 ± 1.8	3.6 ± 2.3
	Synechococcus	2.9 ± 1.5	2.6 ± 1.2
	Eukaryotic algae	0.30 ± 0.15	0.66 ± 0.42
Biomass [g C m^{-2}]	*Prochlorococcus*	**0.37 ± 0.06**	0.18 ± 0.11
	Synechococcus	**0.72 ± 0.16**	0.54 ± 0.18
	Eukaryotic algae	0.72 ± 0.16	**1.37 ± 0.19**
Q_C [fg C $cell^{-1}$]	*Prochlorococcus*	**86 ± 9**	51 ± 10
	Synechococcus	**337 ± 26**	205 ± 37
	Eukaryotic algae	3023 ± 297	3377 ± 287
POC flux [mg C m^{-2} d^{-1}]	150 m	41 ± 19	52 ± 15
	200m	24 ± 10	34 ± 13
	300 m	11 ± 6	21 ± 10
POC:PON flux [mol:mol]	150 m	5.8 ± 0.6	**6.9 ± 0.5**
	200 m	6.3 ± 0.6	**7.8 ± 0.5**
	300 m	7.1 ± 0.7	**8.2 ± 1.0**
T_{eff} [%]	200m/150 m	69 ± 23	76 ± 19
	300m/200 m	42 ± 17	58 ± 14
	300 m/150 m	31 ± 7	43 ± 7

Please cite this article as: Casey, J.R., et al., Changes in partitioning of carbon amongst photosynthetic pico- and nano-plankton groups in the Sargasso Sea in.... Deep-Sea Res. II (2013), http://dx.doi.org/10.1016/j.dsr2.2013.02.002

of which are important to scattering measurements. The sample flow rate at this configuration was 43 ± 18 μL min^{-1}. Where necessary, coincident event detection of ± 1 droplet was used to improve sort purity while maintaining software abort rates below 1%. Regular analysis of sorted populations demonstrated that sort purity was always >95% (calculated as the proportion of sorted events which fell into prescribed gating schema as a percentage of total event rate in sorted sample), and mean recovery from sorted samples was 98.1 ± 1.1% (calculated as the number of target events recovered relative to the number of positive sort decisions recorded by the acquisition software). It should be noted that any sort contamination would have been comprised mainly of particles at or near the forward scatter detection limit, *i.e.*, predominantly very tiny non-cellular particles. Thus, even at ca. 5% contamination by particle count, the POC mass contributed by any contaminant particles would be almost zero, and would not affect the measured Q_C values. We caution that heterotrophic bacteria are routinely observed attached to larger eukaryotic cells (*e.g.*, Cole, 1982) and may result in overestimation of Q_C; however, attached bacteria would presumably also result in higher FSC-H.

Cells were deposited into 5 mL polystyrene Falcon tubes (#352063; BD Biosciences Inc., San Jose, CA) by orienting the side-wall of the tube nearly parallel to the sort stream to reduce unnecessary stress to the sorted cell from deceleration forces. With limited *a priori* knowledge of Q_C values, we conservatively estimated the number of cells needed to exceed twice the minimum mass required for downstream analysis by converting literature-derived *Qc* determinations (Table 1) to cell numbers. Sorts were on the order 10^7 cells for *Prochlorococcus* and *Synechococcus*, 10^5 cells for larger eukaryotic algae. As sufficient yield occasionally required sort times exceeding one hour per population, care was taken to ensure minimal exposure to room temperatures by immediately refrigerating portions of the total sort. Samples were gently filtered (<5 mm Hg) onto either 25 mm 0.2 μm silver (Millipore; for *Prochlorococcus*) or glass fiber filters (GF/F; Whatman; all other sorted chlorophyll-containing cells; nominal 0.7 μm pore size) based upon the size of the cells. Care was taken to ensure a quantitative transfer at this step by performing multiple rinses of the filter tower and sort tube and cap with 0.22 μm filtered artificial seawater to dislodge any 'sticky' cells. Filters were removed with ethanol-cleaned forceps, taking care not to touch the cell deposits, and transferred to pre-combusted 20 ml glass scintillation vials.

2.5.2. Gating

Natural samples were analyzed or sorted for the picocyanobacteria *Prochlorococcus* and *Synechococccus*, and eukaryotic algae. Chlorophyll *a* containing cells were identified and sorted unstained according to a modified gating scheme (Fig. 1). After exclusion of laser noise gated on FSC pulse height (FSC-H) and pulse width (FSC-W), autotrophic cells were identified by red (650 nm long-pass) autofluoresescence. Among the picocyanobacteria, *Synechococcus* was discriminated from *Prochlorococcus* by FSC-H and the presence of yellow/orange (580/30 nm; PE) fluorescence. Chlorophyll containing cells not included in the cyanobacteria gates were assumed to be eukaryotic algae, and sorted as a single group. All post acquisition analysis was performed using FCS Express 3.0 (DeNovo Software, Los Angeles, CA). An identical gating scheme was used for sorting and post acquisition analysis to ensure compatibility.

2.5.3. Osmotic stress experiment

To assess the sensitivity of FSC-H to cell size and Q_C, a simple osmotic stress experiment was designed to alter cell size without

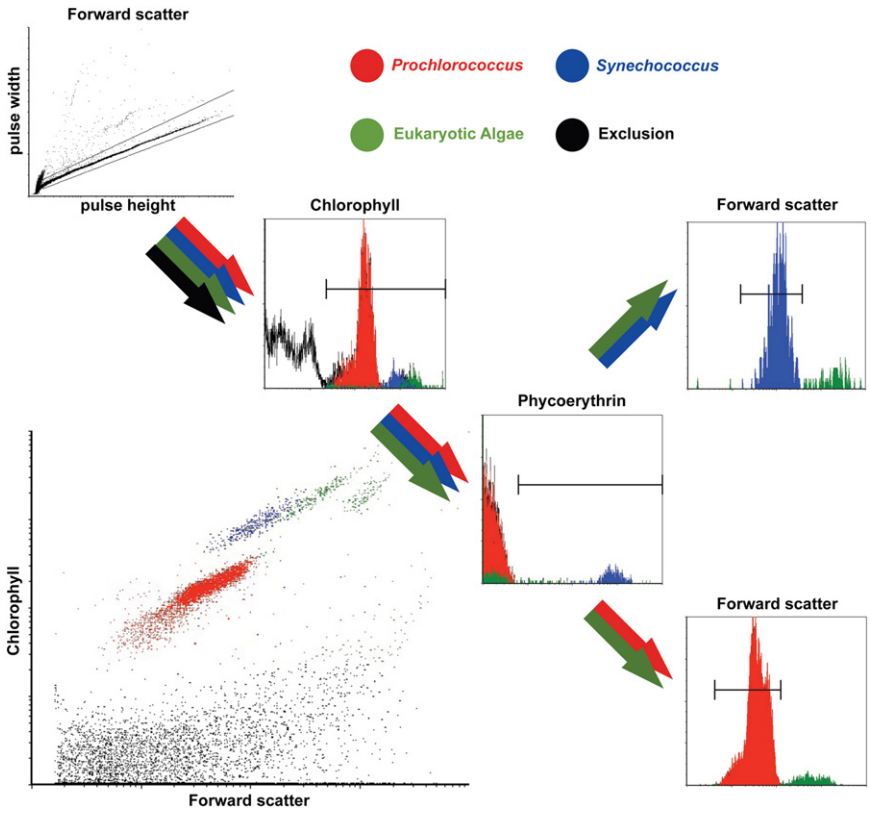

Fig. 1. Phytoplankton gating scheme. Flow diagram illustrating the steps involved in the hierarchical gating of phytoplankton cells from a mixed assemblage. Colored arrows indicate the stepwise filtering of gated events. Events excluding laser noise, electronic noise, and non-particulate events (bubbles) are shown with black arrow. Gates shown in two-dimensional plots, markers in histograms. Inset panel is the resulting cytogram showing all recorded events and gated events in colors.

Please cite this article as: Casey, J.R., et al., Changes in partitioning of carbon amongst photosynthetic pico- and nano-plankton groups in the Sargasso Sea in.... Deep-Sea Res. II (2013), http://dx.doi.org/10.1016/j.dsr2.2013.02.002

influencing Q_C. Duplicate 200 ml samples of Ferry Reach (Bermuda) surface seawater were used. One replicate was dehydrated by fixation (0.5% PFA final concentration) while the other was left alive and each dispensed into nine 5 ml tubes. Live and dead aliquots were diluted with 0.2 μm filter sterilized distilled water or brine (70 ppt NaCl), each at four incremental volume additions. The resulting dilution series varied from 19 ppt to 56 ppt NaCl. Visual inspection by dark-field microscopy displayed intact *Synechococcus*-like cells across all treatments. Using a stage micrometer, live *Synechococcus* cells were 0.8, 1.2, and 1.4 μm in length in hyper-, iso-, and hypo-tonic solutions, respectively. Fixed *Synechococcus* cells were 1.1 μm average length at all salinities.

2.6. Quality and statistical analysis

Quality flagging was set to identify and alert to gated populations which failed the following criteria: events <100, kurtosis <0, skewness -5 to 5. Flagged iterations were discarded from any subsequent analyses in this manuscript. The potential error of non-log-normal population distributions on reported geometric means was estimated using a test described below with mixed populations in a range of concentrations typical to natural Sargasso seawater. Refractive index shifts associated with PFA fixation were accounted for in each cell type by comparing FSC-H between fixed and unfixed cells from laboratory cultures and natural samples.

Data transformations, integrations, statistical tests, time-series analysis and plots were created using MATLAB (The Mathworks, Inc., Natick, MA), R (R-Development Core Team, 2011), or Minitab (Version 15; Minitab Inc., State College, PA). Unless otherwise noted, tests for significant differences were reported according to the two-sample *t*-test assuming unequal variances with number of observations (n) and the p-value. Contour plots were created using Ocean Data View (Version 3) with the weighted average multiple linear interpolation gridding routine. Scatter plots were created using SigmaPlot (Systat Software, Inc., San Jose, CA) and the cyto(histo)grams were created using FCS Express.

3. Results and discussion

3.1. Forward scatter and Q_C

Previous studies have derived cell volume from flow cytometric observations, among other methods (Table 1). Notably, DuRand et al. (2001) compared forward angle light scatter pulse height (FSC-H herein) of target cells to reference beads of known diameter to infer cell diameter as might be predicted by Lorenz–Mie Theory (LMT). Other particle sizing and discrimination techniques have relied on the Rayleigh–Debye–Gans approximation (RDG; *e.g.* Mullaney and Dean, 1969; Barber and Wang, 1978; Holoubek, 1991; Robertson et al., 1998) or the discrete dipole approximation (Rajwa et al., 2008); however, most biological particles in the sea fall outside the boundary conditions required by both LMT and RDG (Ulicny, 1992; Zhao and Ma, 2009; Cucci and Sieracki, 2001). In fact many cellular attributes influence small forward angle light scattering, and these have been reviewed extensively (Salzman et al., 1975; Sharpless et al., 1975; Loken et al., 1976; Sharpless and Melamed, 1976; Shapiro, 1977; Sharpless et al., 1977; Salzman et al., 1979; Kerker, 1983; Salzman et al., 1990; Hoekstra et al., 1994). Specifically, cells are roughly equal in cross-sectional area to the wavelength of incident light (488 nm is the most common laser wavelength), are non-spherical and anisotropic, and have complex internal and surface structure (Aas, 1996; Kerker et al., 1979; Dubelaar et al., 1987). These characteristics are assumed to be zero elements in the Mueller matrix from which both sizing techniques are formulated (Rayleigh, 1910; Petres and Dezelic, 1975; Bickel et al., 1987; Sloot et al., 1989). Further, optical bench designs of commercially available flow cytometers result in non-linear and in some cases non-monotonic size-FSC relationships (Becker et al., 2002). In this study a direct method of comparing FSC-H to POC was employed.

Experimental measurements of Q_C were highly correlated to FSC-H (normalized to 0.53 μm beads) over a wide size range (approximate diameter 0.2 μm–12 μm; $Q_C = 99.14 \times \text{FSC-H} + 15.11$; $r^2 = 0.994$; $n = 24$; ANOVA; $D_f = 22$, $p = 2.2\text{e-}16$; Fig. 2). The ordinal intercept of this empirically derived calibration curve was not significantly different from zero ($dF = 22$; $t = 0.312$; SE = 158.8; $p = 0.758 > p_{crit} = 0.05$). All live cells, whether harvested from laboratory cultures or natural samples, and regardless of growth condition followed the same linear regression relationship suggesting over this range of cell sizes and growth conditions a near constant carbon per unit biovolume. It should be noted that the cell shapes included in the calibration curve were limited to coccoid or bacilliform and should not be extended to spirilli, filamentous, or more complex arrangements. Because elemental analysis was performed on unfixed cells, a correction factor was applied to the calibration curve to account for dehydration effects on refractive index associated with fixation by paraformaldehyde. Fixed natural populations of *Prochlorococcus*, *Synechococcus*, eukaryotic algae showed a 6.5% reduction in FSC-H relative to live cells ($n = 20$, $r^2 = 0.9998$; Fig. 3A); this correction was applied to the slope of the calibration function. Changes in the applied voltage gain (11 to 76 arbitrary units) to photomultiplier tubes and log-preamplifiers did not introduce any noticeable artifacts to the determination of forward scatter amplitude over the dynamic range relevant to this study (26 to 34 arbitrary units; $n = 56$, $r^2 = 0.997$; Fig. 3B).

Experimental observations of cells altered in size but not Q_C (via osmotic manipulations; Section 2.5.3) recorded statistically identical slopes of FSC-H as a function of salinity for live *Synechococcus* cells between 0.8 μm and 1.4 μm when compared to 1.1 μm fixed *Synechococcus* cells which did not vary in size with salinity ($n = 16$, $p < 0.0001$; Fig. 3C). It is important to note that the effects on FSC-H by mismatched refractive indices between sheath and sample core (Cucci and Sieracki, 2001) and fixative (this study) were accounted for in this experiment. FSC-H was therefore sensitive to changes not only in absolute cell size but also to changes in Q_C independent of cell size changes, at least for picophytoplankton of similar size as *Synechococcus*, highlighting

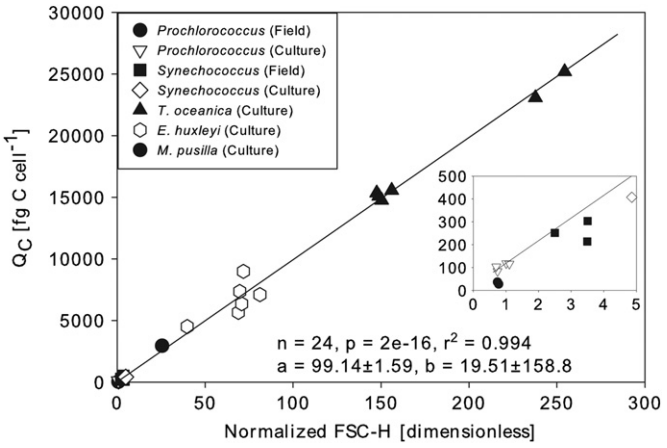

Fig. 2. Calibration curve. Average Q_C as a function of geometric mean forward scatter pulse height for the population sorted and normalized to peak value of 0.53 μm polystyrene calibration particles. Inset blow-up panel shows lower range of data distribution. Model I linear regression (solid line), coefficient of determination (R^2), number of observations (n), slope (a) and intercept (b) are shown. Error bars represent one standard deviation of the mean.

Please cite this article as: Casey, J.R., et al., Changes in partitioning of carbon amongst photosynthetic pico- and nano-plankton groups in the Sargasso Sea in.... Deep-Sea Res. II (2013), http://dx.doi.org/10.1016/j.dsr2.2013.02.002

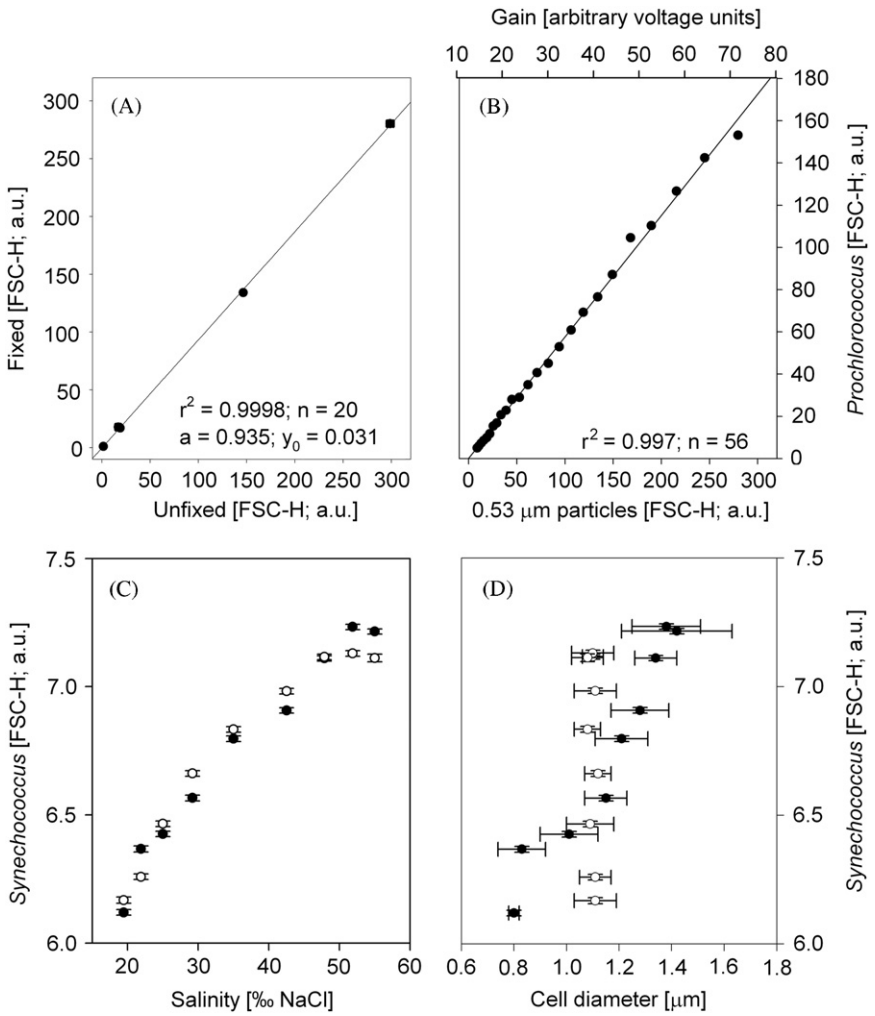

Fig. 3. Method validations. (A) A 6.5% refractive index shift (n) was associated with paraformaldehyde fixation on *Prochlorococcus*, *Synechococcus*, *Thallasiosira oceanica*, and *Emiliana huxleyi* cultures and natural populations of *Prochlorococcus*, *Synechococcus* and two subpopulations of eukaryotic algae. Parameters for Model I least squares linear regression (solid line): r^2—coefficient of determination, n—number of observations, a—slope of regression, y_0—intercept. (B) Linearity of FSC-H normalization to 0.53 μm calibration particles under various instrument gain settings. Photomultiplier tube voltage and log preamplifiers did not introduce any non-linearity over the range of gain settings used throughout this study. Linear regression shown as solid line. (C) Osmotic stress experiment (see details in Section 2.5.3). Influence of live (closed symbols) and fixed (open symbols) *Synechococcus* cells exposed to a series of hyper-, iso-, and hypo-tonic solutions on FSC-H (normalized to 0.53 μm calibration particles). Error bars represent one standard error. PFA fixed cells were corrected for refractive index shift (n) as in (A). (D) FSC-H data from (C) reploted as a function of cell diameter. Scattering amplitude was influenced by mismatched refractive indices rather than the associated changes in cell size.

the distinction between cellular volume and Q_C. It is concluded that scattering matrix elements required by Mueller's matrix for ideal scatterers are not appropriate for biological particles with cross sectional diameters similar to incident light wavelengths. Thus picophytoplankton are not suitable candidates for direct flow cytometry based sizing techniques. An inverse solution to the Mueller matrix, specific to our optical bench design and fluidics, would be required to evaluate the sensitivity of particle cross-sectional area beyond the extremes of the linear range of our calibration curve. Regardless, these observations confirm the utility of FSC-H estimates of Q_C within the pico/nanophytoplankton size range.

3.2. Taxon specific Q_C

In natural samples of *Prochlorococcus* and *Synechococcus*, log-normal distributions in FSC-H histograms were typical (kurtosis >1, skewness -5 to 5) and central tendency metrics (geometric mean, median, peak value) were often indistinguishable, a strong indication of log-normal distribution. Eukaryotic algae gates were sometimes of complex modality or skewed due to the presence of multiple populations or no clearly dominant population. The potential error associated with irregular FSC-H distributions was calculated by comparing geometric mean and median values of cumulative sum bins at a series of decreasing logarithmic bin sizes ($k=1$ to $k=1000$). Using this approach, and given the tolerances of our flagging criteria, it was estimated that a random FSC-H distribution would introduce no more than 2% error to the eukaryotic algae community POC calculation. Random distributions were infrequent; log-normal distributions for eukaryotes satisfied the flagging criteria and coefficient of variation was better than 15% in 93% of samples where more than 100 events were recorded. Unless noted otherwise, average Q_C values are reported in three depth intervals (0–40, 60–120, 140–250 m). These horizons were chosen according to a variety of environmental parameters; specifically, 40–60 m was chosen as the approximate inflection in both *Prochlorococcus* and *Synechococcus* abundance profiles during the stratified period (April through November); 120 m was chosen as the approximate depth of the 1% PAR isolume delimiting the euphotic and sub-euphotic layers.

Q_C typically increased in the order *Prochlorococcus*, *Synechococcus*, and eukaryotic algae; however, considerable overlap within

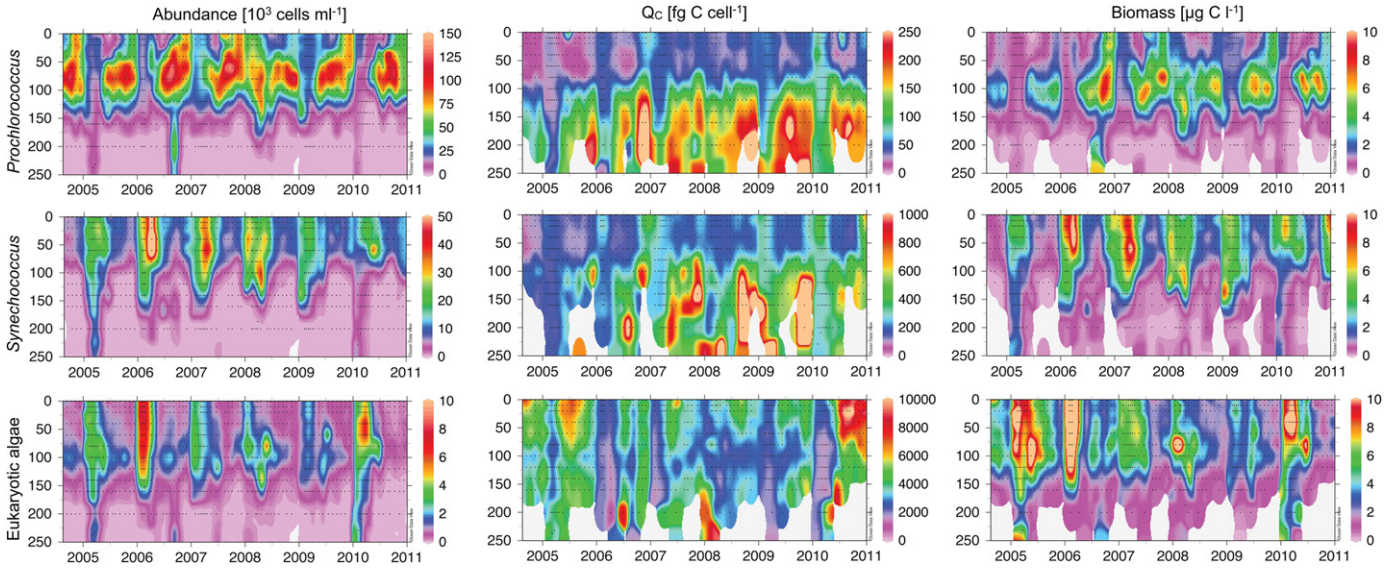

Fig. 4. Flow cytometry derived parameters. Contour plots of cellular abundance (left column panels), Q_C (middle column panels), and biomass (right column panels) for *Prochlorococcus* (top row panels), *Synechococcus* (middle row panels), and eukaryotic algae (bottom row panels). Missing data or data which failed the statistical tests (as described in Section 2.6) are shown in white.

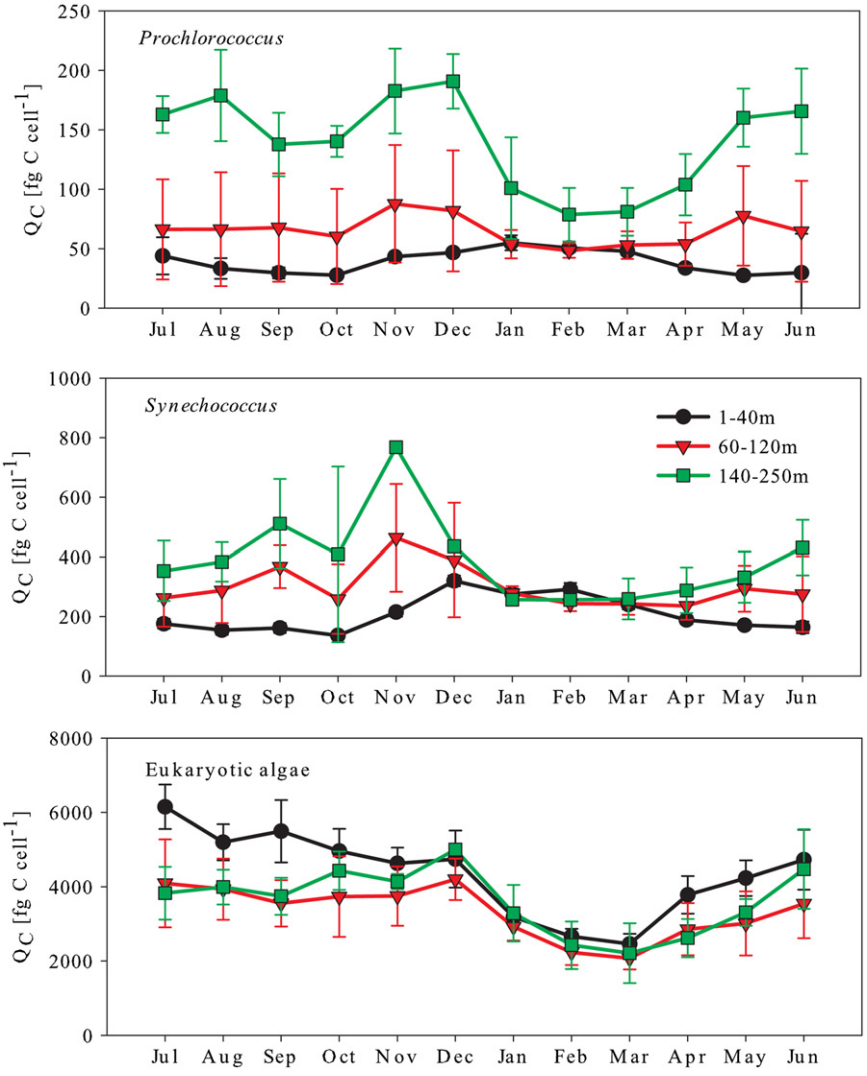

Fig. 5. Seasonality of Q_C. Q_C for each phytoplankton group averaged over three depth intervals for all years. Error bars represent one standard deviation from the mean.

Please cite this article as: Casey, J.R., et al., Changes in partitioning of carbon amongst photosynthetic pico- and nano-plankton groups in the Sargasso Sea in.... Deep-Sea Res. II (2013), http://dx.doi.org/10.1016/j.dsr2.2013.02.002

individual samples was observed between groups depending upon the various growth conditions highlighting the benefits of taxonomic rather than size fractionation based separation techniques for physiological studies. Mean Q_C values for all groups were within the range of values previously reported using a variety of other techniques (Table 1). Importantly, variability of Q_C for individual samples spanned more than an order of magnitude within each taxonomic group through all temporal and spatial scales available in this dataset, emphasizing the error introduced to biomass measurements reliant on fixed abundance-to-carbon conversion factors.

Seasonally from January to December, *Prochlorococcus* Q_C values generally decreased in the upper 40 m whereas at the deeper depth ranges, Q_C values increased. *Prochlorococcus* Q_C varied from a low of 28 ± 2 fg C cell^{-1} in January in the upper 40 m to a high of 190 ± 23 fg C cell^{-1} in December below 140 m (Fig. 5). A portion of this Q_C increase was likely due to increased thylakoid membrane surface area needed to support increased cellular chlorophyll and accessory pigments in response to low light, perhaps pointing to the role of ecotype-specific photophysiologies in controlling Q_C. Low light adapted strains of *Prochlorococcus* tightly pack thylakoid membranes at the periphery of the cytoplasm, a photophysiological strategy that contributes to a strong "packaging effect" (Partensky et al.,1993). A persistent inflection in Q_C at 40–80 m, perhaps due to a shift in dominance from high-light to low-light ecotypes, as observed by Malmstrom et al. (2010) and Moore and Chisholm (1999), supports this observation. Furthermore, we observed that depth dependent decreases in the FSC-H to red fluorescence intensity ratio (indicative of the C:chl ratio; data not shown) tended to be lower for *Prochlorococcus* compared with *Synechococcus* and the eukaryotes.

Like *Prochlorococcus*, annually averaged *Synechococcus* Q_C increased with depth from 197 ± 16 fg C cell^{-1} above 40 m to 386 ± 140 fg C cell^{-1} below 140 m. This increase in Q_C with depth was consistently less dramatic (ca. 2-fold) than *Prochlorococcus* (often more than 5-fold) over the same depth interval. Perhaps the limited depth range of *Synechococcus*, the presence of multiple co-occurring ecotypes and the absence of a physiologically distinct low light-adapted ecotype (Ahlgren and Rocap, 2006) can explain the reduced depth-dependent variability of Q_C in *Synechococcus*. Contrary to *Prochlorococcus*, within the spring "bloom" in the upper 40 m, average *Synechococcus* Q_C was significantly higher (291 ± 22 fg C cell^{-1}) compared to the rest of the year (136 ± 6 fg C cell^{-1}; $n=1071$, $p=0.012$; Fig. 5B).

Surprisingly, eukaryotic algae were the most consistent group with respect to Q_C within each depth range showing a coherent seasonal increase from minima in the spring to maxima in the summer/fall. This uniformity is likely an effect of averaging high diversity. A persistent Q_C minimum appeared to be associated with the 1–10% PAR isolume during the stratified period (June through November; 5011 ± 1857, 3793 ± 1350, 4121 ± 1263 fg C cell^{-1} for 0–40, 60–120, 140–250 m; Welch's two sample *t*-test; $t=-1.92$, d*f*$=160$, $p=0.05$).

3.3. Seasonal algal biomass dynamics

Autotrophic biomass was calculated as the product of Q_C and cell abundance. Summed over the three groups, integrated photosynthetic biomass ($\int$0–250 m) was 34 ± 16% of bottle POC (captured on a GF/F, nominal pore size 0.7 μm); 90% of which was restricted to the upper 120 m. Fig. 6 Large (>12 μm) algae were independently determined to contribute at most 5–10% of integrated autotrophic POC annually but often much less (Priyadarshani and Lomas, unpublished data). Although all particles <35 μm are detected by the flow cytometer, the dynamic range of forward scatter was optimized for pico/nanophytoplankton. With the instrument settings used in this study, PMT voltage and volume analyzed, we could not discriminate cells between ca. 12 μm and 35 μm, and cells in this size range are grouped together in the largest size bin (pixel column) in cytograms. However, we note qualitatively that nanoeukaryotic algae in the largest size bin (>12 μm) were rare. With this caution, average photosynthetic biomass during the winter (Dec, Jan, Feb) period was half of bottle POC in the euphotic zone (48 ± 9% from 0–40 m; 48 ± 7% from 60–120 m) and 35 ± 14% in the sub-euphotic zone (140–250 m; data not shown). In contrast, vertical structure in photosynthetic biomass was apparent throughout the rest of the year (March through November) with 28 ± 8, 42 ± 7, and 29 ± 7% of total POC in the 0–40, 60–120, and 140–250 m depth intervals, respectively. It is interesting to note that our formulation of photosynthetic carbon biomass showed a significant local maximum (Welch's two sample *t*-test; $t=1.95$, d*f*$=451$, $p=0.05$) coincident with the deep chlorophyll maximum depth interval (60–120 m) during this stratified period. For the duration of the *Prochlorococcus* numerical maximum (May through November) the subsurface photosynthetic carbon biomass maximum was roughly 50% higher than the 0–40 m interval ($t=6.83$, d*f*$=305$, $p=4.7\text{e-}11$). This finding is in direct conflict with current dogma that the deep chlorophyll maximum at BATS is a pigment maximum but not a maximum in photosynthetic biomass.

DuRand et al. (2001) provide an extensive review of seasonal phytoplankton abundance dynamics at the BATS site that is, to a great extent, appropriate for our study period. *Prochlorococcus* cell concentrations showed seasonal maxima in October at $9.8 \pm 1.3 \times 10^{12}$ cells m^{-2}. A persistent subsurface maximum appeared to be closely associated with the nitracline, an observation often reported (Olson et al., 1990; Lindell and Post, 1995; DuRand et al., 2001). A subsurface maximum also reflects the low optimal growth irradiances of low-light adapted ecotypes of *Prochlorococcus* relative to *Synechococcus* (Morel et al., 1993).

Ecotypes within the *Prochlorococcus* subsurface abundance maximum assemblage appeared to be unable to cope with turbulent, deep winter mixing as evidenced through decreases in population sizes coinciding with these events (Fig. 4). As an extreme example, during the strong mixing event of 2010 where mixed layers were >400 m, *Prochlorococcus* abundance decreased to 0.3×10^{12} cells m^{-2} and 0.02 g C m^{-2} implying 88% mortality within only a two week period and 97% mortality during the entire 3 month mixing period. Because >90% of the *Prochlorococcus* population directly preceding the decline was found below the 10% PAR isolume, we may infer that low light adapted ecotypes (LL) eroded during winter mixing were selectively eliminated. Although average light intensity within the mixed layer was reduced, low light acclimated populations experienced high light field exposure, if even for brief periods. Thus, possible causes for mortality may be: (1) grazing, (2) the absence of photolyase UV repair mechanisms in LL *Prochlorococcus* and thus limited photophysiological ability to respond to exposure to increased light fields (Ting et al., 2002; Rocap et al., 2003), (3) viral lysogeny (Parsons et al., 2011), (4) sensitivity of LL *Prochlorococcus* to copper toxicity (Mann et al., 2002) or interestingly, (5) copper induced viral lysis (Sode et al., 1997). Alternatively, Lomas and Moran (2010) offer aggregation and repackaging as potential mechanisms for the export of picocyanobacteria at the BATS site but the magnitude of annual *Prochlorococcus* disappearance is not resolved in sediment traps indicated by pigment analysis (5 ± 7% of C export; Lomas and Moran, 2010) or by molecular fingerprinting (<5.7%; Amacher, 2011).

Strong niche partitioning between *Prochlorococcus* and *Synechococcus* was apparent both in depth profiles and seasonal dynamics. *Synechococcus* abundance maxima were strictly within the upper 80 m, directly above the *Prochlorococcus* abundance maximum. Seasonally, *Synechococcus* were most abundant in April ($4.4 \pm 2.6 \times 10^{12}$ cells m^{-2}), decreasing steadily through late

Please cite this article as: Casey, J.R., et al., Changes in partitioning of carbon amongst photosynthetic pico- and nano-plankton groups in the Sargasso Sea in.... Deep-Sea Res. II (2013), http://dx.doi.org/10.1016/j.dsr2.2013.02.002

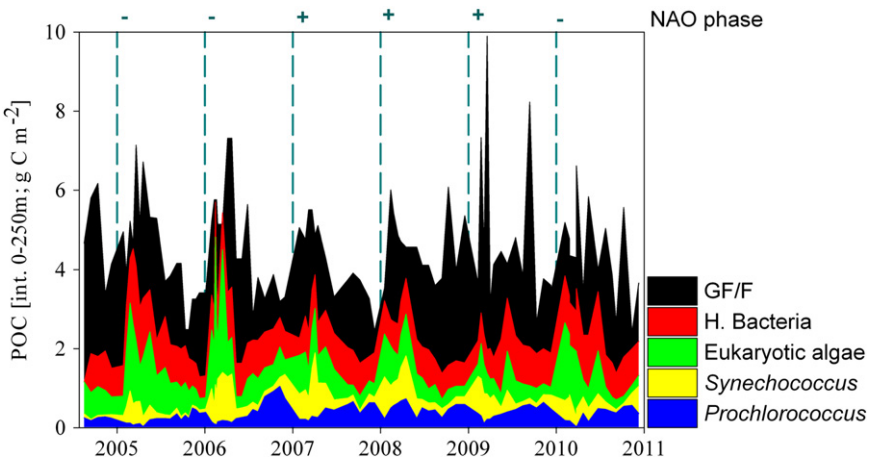

Fig. 6. Microbial carbon. Cumulative area plot of *Prochlorococcus*, *Synechococcus*, eukaryotic algae and heterotrophic bacteria biomass overlaid on total POC (GF/F). Unidentified POC shown in black. NAO phase shown as "+" or "−" at the start of each year along the top.

fall ($0.58 \pm 0.07 \times 10^{12}$ cells m^{-2} in October). Divergence of temperature optima, nutritional requirements and preference, photophysiological adaptations and other growth strategies between these closely related cyanobacteria may help to explain seasonal and biogeographical distributions (*e.g.*, Morel et al., 1993; Partensky et al., 1999). Contrary to *Prochlorococcus*, viral control does not appear to be important for *Synechococcus* at BATS (Parsons et al., 2011), pointing to nutrient availability as a likely constraint on biomass. Species competition for orthophosphate and hydrolyzable DOP may be particularly important at the BATS site where soluble reactive phosphorus is perpetually below 10 nmol l^{-1} in the stratified upper 100 m (Lomas et al., 2010). High alkaline phosphatase activities (Torres-Valdes et al., 2009; Lomas et al., 2010) and rapid turnover of the SRP pool (3–5 h; Ammerman et al., 2003) imply that differences in inorganic phosphate affinity and cleavage from hydrolyzable DOP between taxa are important determinants of community structure at the BATS site. Absolute and biomass normalized orthophosphate assimilation rates were higher in *Synechococcus* than *Prochlorococcus* (Casey et al., 2009) and picocyanobacteria were more efficient at scavenging and assimilating orthophosphate from ^{33}P-labeled adenosine triphosphate compared to eukaryotic algae. It is therefore likely that *Synechococcus* P-specific growth rates are simply higher than HL *Prochlorococcus* throughout the upper euphotic zone during winter mixing periods when SRP concentrations can exceed 20 nmol l^{-1}. *Prochlorococcus* subsequently occupies the 1–10% PAR layer where light intensities are suitable for low light adapted ecotypes.

Seasonal population dynamics and depth distributions of eukaryotic algae were far more complex than *Prochlorococcus* and *Synechococcus*. Frequently, two to three discrete populations were detected in a single profile, and gated events not necessarily associated with the dominant populations were relatively less abundant (7 ± 3% and 30 ± 25% of total eukaryotic algae abundance) above than below 60 m, respectively. These larger red fluorescing cells are diverse taxonomically (Díez et al., 2001; López García et al., 2001), and molecular approaches (*e.g.*, Not et al., 2007) to characterizing these organisms continue to improve our understanding of the composition and function of the picoeukaryotic algae (Worden et al., 2004; Worden and Allen, 2010). Seasonally, eukaryotic algal abundance maximum followed the DCM through late summer and fall coincident with the *Prochlorocccus* deep abundance maximum. Smaller (<2000 fg C $cell^{-1}$) eukaryotes belonging to a single cytometric population were first to bloom following winter mixing; eukaryotic algae abundance maximum was during February ($0.70 \pm 0.43 \times 10^{12}$ cells m^{-2}). Taking in to account the complex nature of the eukaryotic algae, integrated abundance decreased through late fall with numerical minima occurring in November ($0.11 \pm 0.05 \times 10^{12}$ cells m^{-2}) similar to *Synechococcus*.

3.4. Influence of NAO on winter algal community structure

In addition to seasonal abundance and Q_C, interannual variability in monthly pico/nanophytoplankton biomass was significantly higher ($n=506$, $p=0.02$) during late winter (January-March) than the rest of the year. A similar trend was observed in monthly mixed layer depth with interannual variability highest during January and February ($n=136$, $p=2e\text{-}16$). In the North Atlantic Subtropical Gyre (NASG), the dominant climate mode influencing interannual trends in winter sea surface temperature (SST), storm trajectory, and mixed layer depth is the North Atlantic Oscillation (NAO; Rodwell et al., 1999; Visbeck et al., 2001; Wang et al., 2004; Hurrell and Deser, 2009). Correspondingly, the amplitude of the NAO signal is highest in winter in our study region (Visbeck, et al., 2001; Wang et al., 2004). The sea level pressure gradient between Iceland and the Azores (NAO) is driven primarily by variability in the strength of the North Atlantic subtropical high (also known as the Azores or Bermuda high) pressure system and oscillates at an approximate period of 8 years (García et al., 2005). During NAO positive regimes a strong Iceland–Azores pressure gradient draws a southwesterly flow of warm dry/wet air originating over the southeastern United States. This feature blocks arctic flow from reaching the US east coast and shifts storm tracks northward to favor calmer winters, lower sea surface salinity (SSS), warmer sea surface temperature (SST) and consequently weaker (both in magnitude and duration) convective mixing near Bermuda (Hurrell and Deser, 2009). Conversely, NAO negative years weaken the Iceland–Azores pressure gradient allowing Arctic flow and directing winter storm tracks toward Bermuda. Thus in NAO negative winters, Bermuda experiences intensified northerlies and northeasterlies, and frequent passage of cold fronts resulting in accelerated ocean-atmosphere heat exchange, southerly expansion of the site of mode water formation (surface ventilation of 18 °C isotherm) and enhanced penetration of the mixed layer through the 1% photosynthetically active radiation (PAR) isolume and nutricline. Physical conditions associated with deep convective mixing and subsequent entrainment of nutrients into the euphotic zone is anticipated to collectively influence algal community activity and composition but not necessarily numerical abundance (*e.g.*, Margalef, 1978).

Please cite this article as: Casey, J.R., et al., Changes in partitioning of carbon amongst photosynthetic pico- and nano-plankton groups in the Sargasso Sea in.... Deep-Sea Res. II (2013), http://dx.doi.org/10.1016/j.dsr2.2013.02.002

Total POC and chlorophyll *a* standing stocks during the winter period were not significantly different between NAO modes ($p=0.383$, 0.544, respectively, Table 2). Total autotrophic POC, bacterial and "unidentified" biomass were also statistically identical each winter ($p=0.835$, 0.524, 0.113, respectively). However, striking changes in mixed layer depth maxima, phytoplankton community composition and Q_C correlated with the NAO phase (Table 2). We also noticed changes in the magnitude, particulate elemental stoichiometry, and transfer efficiency of the carbon and nitrogen export flux associated with the NAO (Table 2).

During NAO positive winters, picocyanobacterial biomass dominated total autotrophic biomass as compared to NAO negative winters ($60\pm15\%$, $n=316$, $p=0.026$). Simultaneously, picocyanobacterial Q_C was elevated (86 ± 9 and 337 ± 26 fg C cell^{-1} for *Prochlorococcus* and *Synechococcus*, respectively) compared with NAO negative years (51 ± 10 and 205 ± 37 fg C cell^{-1}, respectively). Conversely, during negative NAO winters pico/nanoeukaryotic algae became the dominant portion ($66\pm9\%$) of total autotrophic biomass as compared to NAO positive winters ($n=301$, $p=0.021$); during these winters eukaryotic algae Q_C tended to be higher (3377 ± 287 fg C cell^{-1}) than during NAO positive regimes (3023 ± 297 fg C cell^{-1}), though not significantly ($n=301$, $p=0.186$). As NAO negative winters were aligned with the deepest mixing periods, we infer that enhanced nutrient injection and reduced light intensity was responsible for the success of eukaryotic algae. This finding is consistent with current understanding of the influence of NAO on hydrographic conditions at the BATS site (Bates, 2001) as well as changes in plankton community structure associated with NAO (Irigoien et al., 2000; Lomas et al., 2004; Lomas et al., 2009). Importantly, no significant difference was observed between NAO regimes using counts alone and therefore taxon-specific biomass trends to NAO index would have been overlooked if a fixed conversion factor were used.

4. Conclusions

Findings from this study (1) demonstrate systematic variability in Q_C as a function of depth and through time and (2) reveal sensitivity of phytoplankton community composition to hydrographic conditions governed by interannual changes in climatology. We conclude that the NAO plays an important role in shaping winter phytoplankton assemblage composition, particle export flux characteristics, and subsequently the efficiency of the biological carbon pump. When interpreting long-term temporal trends, the location of the BATS site should be considered in the context of the spatial extent, overlap and superposition of adjacent water masses. Hydrographic changes associated with climate oscillations are probably implicit to all open ocean Eulerian-type time-series, and so autotrophic biomass estimates may prove useful in describing biogeographical regions (or 'biomes') confined by geophysical boundaries in both diagnostic and prognostic models (*e.g.*, Follows and Dutkiewicz, 2011). In addition to regional oscillations like NAO, smaller amplitude, longer period climate modes (*e.g.*, Atlantic Multi-decadal Oscillation) and secular change are expected to influence algal community structure. Although the BATS flow cytometric picophytoplankton record does not currently extend far enough into the past to provide meaningful insights, taxonomically resolved records of biomass will be useful in the future for identifying subtle interannual climate signals.

Acknowledgments

We are grateful to the BATS technical staff and the captains and crew of the R/V Atlantic Explorer and R/V Weatherbird II for their support. Special thanks to R. Parsons, S. Allender, and K. Lew for their assistance with bacteria counts and elemental analysis measurements. Thanks to R. Johnson, D. Evans, and N. McDonald for kindly providing updated quality-controlled BATS data presented in this manuscript. This research was supported by NSF awards OCE-0420821 and OCE-1045966 to MWL. We also acknowledge NSF support of the BATS program via recent awards OCE-0326885 and OCE-0752366. This is BIOS contribution number 2024.

References

Aas, E., 1996. Refractive index of phytoplankton derived from its metabolite composition. J. Plankton Res. 18, 2223–2249.

Ahlgren, N., Rocap, G., 2006. Culture isolation and culture-independent clone libraries reveal new marine *Synechococcus* ecotypes with distinctive light and N physiologies. Appl. Environ. Microbiol. 72, 7193–7204.

Amacher, J., 2011. Protist and cyanobacterial contributions to particle flux in oligotrophic ocean regions. Ph.D. Thesis. Arizona State University.

Ammerman, J.W., Hood, R.R., Case, D., Cotner, J.B., 2003. Phosphorus deficiency in the Atlantic: an emerging paradigm in oceanography. EOS 84, 164–170.

Barber, P.W., Wang, D.-S., 1978. Rayleigh–Gans–Debye applicability to scattering by nonspherical particles. Appl. Opt. 17, 797–803.

Bates, N., 2001. Interannual variability of oceanic CO2 and biogeochemical properties in the Western North Atlantic subtropical gyre. Deep–Sea Res. II 48, 1507–1528.

Becker, A., Meister, A., Wilhelm, C., 2002. Flow cytometric discrimination of various phycobilin-containing phytoplankton groups in a hypertrophic reservoir. Cytometry 48, 45–57.

Bertilsson, S., Berglund, O., Karl, D.M., Chisholm, S.W., 2003. Elemental composition of marine *Prochlorococcus* and *Synechococcus*: implications for the ecological stoichiometry of the sea. Limnol. Oceanogr. 48, 1721–1731.

Bickel, W.S., Watkins, A.J., Videen, G., 1987. The light-scattering Mueller matrix elements for Rayleigh, Rayleigh-Gans and Mie spheres. Am. J. Phys. 55, 559–561.

Blanchot, J., Rodier, M., 1996. Picophytoplankton abundance and biomass in the western tropical Pacific Ocean during the 1992 El Nino year: results from flow cytometry. Deep–Sea Res. Part I 43, 877–895.

Buitenhuis, E.T., Li, W.K.W., Vaulot, D., Lomas, M.W., Landry, M., Partensky, F., Karl, D.M., Ulloa, O., Campbell, L., Jacquet,S., Lantoine, F., Chavez, F., Macias, D., Gosselin, M., McManus, G.B. Picophytoplankton biomass distribution in the global ocean. Earth Syst. Sci. Data Discuss., in press.

Cailliau, C., Claustre, H., Vidussi, F., Marie, D., Vaulot, D., 1996. Carbon biomass, and gross growth rates as estimated from ^{14}C pigment labelling, during photoacclimation in *Prochlorococcus* CCMP 1378. Mar. Ecol. Prog. Ser. 145, 209–221.

Campbell, L., Nolla, H., Vaulot, D., 1994. The importance of *Prochlorococcus* to community structure in the central North Pacific Ocean. Limnol. Oceanogr. 39, 954–961.

Casey, J.R., Lomas, M.W., Mandecki, J., Walker, D.E., 2007. *Prochlorococcus* contributes to new production in the Sargasso Sea deep chlorophyll maximum. Geophys. Res. Lett. 34, L10604.

Casey, J.R., Lomas, M.W., Michelou, V.K., Dyhrman, S.T., Orchard, E.D., Ammerman, J.W., Sylvan, J.B., 2009. Phytoplankton taxon-specific orthophosphate (Pi) and ATP utilization in the western subtropical North Atlantic. Aquat. Microb. Ecol. 58, 31–44.

Chen, B., Tadonléké, R., Llopiz, J., Ballantyne IV, F., Nakayama, K., Souza, M., Savage, C., Holtgrieve, G., Buchwald, C., Vaquer-Sunyer, R., 2010. Relationships between phytoplankton growth and cell size in surface oceans: interactive effects of temperature, nutrients, and grazing. Limnol. Oceanogr. 55, 965–972.

Chisholm, S.W., 1992. Phytoplankton Size. In: Falkowski, P.G. (Ed.), Primary Productivity and Biogeochemical Cycles in the Sea. Springer.

Claustre, H., Bricaud, A., Babin, M., Bruyant, F., Guillou, L., Le Gall, F., Marie, D., Partensky, F., 2002. Diel variations in Prochlorococcus optical properties. Limnol. Oceanogr. 47, 1637–1647.

Cole, J.J., 1982. Interactions between bacteria and algae in aquatic ecosystems. Annu. Rev. Ecol. Syst. 13, 291–314.

Cucci, T., Sieracki, M., 2001. Effects of mismatched refractive indices in aquatic flow cytometry. Cytometry 44, 173–178.

Curry, R., McCartney, M., Joyce, T.M., 1998. Oceanic transport of subpolar climate signals to mid-depth subtropical waters. Nature 391, 575–577.

Díez, B., Pedros-Alio, C., Massana, R., 2001. Study of genetic diversity of eukaryotic picoplankton in different oceanic regions by small-subunit rRNA gene cloning and sequencing. Appl. Environ. Microbiol. 67, 2932–2941.

Dubelaar, G.B.J., Visser, J.W.M., Donze, M., 1987. Anomalous behavior of forward and perpen-dicular light-scattering of a cyanobacterium owing to intracellular gas vacuoles. Cytometry 8, 405–412.

Dunne, J.P., Gnanadesikan, A., Sarmiento, J.L., Slater, R., 2010. Technical description of the prototype version (v0) of Tracers of Phytoplankton with Allometric Zooplankton (TOPAZ) ocean biogeochemical model as used in the Princeton IFMIP model. Biogeosciences 7, 3593.

DuRand, M., Olson, R., Chisholm, S.W., 2001. Phytoplankton population dynamics at the Bermuda Atlantic Time-series station in the Sargasso Sea. Deep–Sea Res. II 48, 1983–2003.

Fawcett, S.E., Ward., B.B., 2011. Phytoplankton succession and nitrogen utilization during the development of an upwelling bloom. Mar. Ecol. Prog. Ser. 428, 13–31.

Follows, M.J., Dutkiewicz, S., 2011. Modeling diverse communities of marine microbes. Annu. Rev. Mar. Sci. 3, 427–451.

Fuhrman, J., Sleeter, T., Carlson, C.A., Proctor, L., 1989. Dominance of bacterial biomass in the Sargasso Sea and its ecological implications. Mar. Ecol. Prog. Ser. 57, 207–217.

García, N., Gimeno, L., La Torre, L., Nieto, R., Anel, J., 2005. North Atlantic Oscillation (NAO) and precipitation in Galicia (Spain). Atmósfera 18, 25–32.

Garrison, D., Gowing, M., Hughes, M., Campbell, L., Caron, D., Dennett, M., Shalapyonok, A., Olson, R., Landry, M., Brown, S.L., 2000. Microbial food web structure in the Arabian Sea: a US JGOFS study. Deep–Sea Res. II 47, 1387–1422.

Grob, C., Ulloa, O., Claustre, H., Huot, Y., Alarcón, G., Marie, D., 2007. Contribution of picoplankton to the total particulate organic carbon concentration in the eastern South Pacific. Biogeosciences 4, 837–852.

Guillard, R.R.L., 1983. Culture of phytoplankton for feeding marine invertabrates. In: Berg, C.J. (Ed.), Culture of Marine Invertebra: Selected Readings. Hutchinson Ross Publishing, Stroudsberg, pp. 108–132.

Halliwell Jr, G., Cornillon, P., 1990a. Large-scale SST variability in the western North Atlantic Subtropical Convergence Zone during FASINEX. Part I: Description of SST and wind stress fields. J. Phys. Oceanogr. 20, 209–222.

Halliwell Jr, G., Cornillon, P., 1990b. Large-scale SST variability in the western North Atlantic subtropical convergence zone during FASINEX. Part II: Upper ocean heat balance and frontogenesis. J. Phys. Oceanogr. 20, 223–234.

Hanson, H.P., Cornillon, P., Halliwell Jr., G.R., Halliwell, V., 1991. Climatological Perspectives, Oceanographic and Meteorological, on Variability in the Subtropical Convergence Zone in the Northwestern Atlantic. J. Geophys. Res. 96, 8517–8529.

Heldal, M., Scanlan, D., Norland, S., Thingstad, F., Mann, N., 2003. Elemental composition of single cells of various strains of marine *Prochlorococcus* and *Synechococcus* using X-ray microanalysis. Limnol. Oceanogr. 48, 1732–1743.

Hoekstra, A., Doornbos, R., Deurloo, K., Noordmans, H., Grooth, B., Sloot, P., 1994. Another face of Lorenz-Mie scattering: monodisperse distributions of spheres produce Lissajous-like patterns. Appl. Opt. 33, 494–500.

Holm-Hansen, O., Riemann, B., 1978. Chlorophyll a determination: improvements in methodology. Oikos 30, 438–447.

Holoubek, J., 1991. Small-angle light scattering from an anisotropic sphere in the Rayleigh-Gans-Debye approximation: the Mueller matrix formalism. Appl. Opt. 30, 4987–4990.

Huot, Y., Babin, M., Bruyant, F., Grob, C., Twardowski, M., Claustre, H., 2007. Relationship between photosynthetic parameters and different proxies of phytoplankton biomass in the subtropical ocean. Biogeosciences 4, 853–868.

Hurrell, J.W., Deser, C., 2009. North Atlantic climate variability: the role of the North Atlantic Oscillation. J. Mar. Syst 78, 28–41.

Irigoien, X., Harris, R., Head, R., Harbour, D., 2000. North Atlantic Oscillation and spring bloom phytoplankton composition in the English Channel. J. Plankton Res. 22, 2367.

Ishizaka, J., Kiyosawa, H., Ishida, K., Ishikawa, K., Takahashi, M., 1994. Meridional distribution and carbon biomass of autotrophic picoplankton in the Central North Pacific Ocean during late northern summer 1990. Deep–Sea Res. I 41, 1745–1766.

Kana, T.M., Glibert, P.M., 1987. Effect of irradiances up to 2000 $\mu E\ m^{-2}\ s^{-1}$ on marine Synechococcus WH7803 – I. Growth, pigmentation, and cell composition. Deep–Sea Res. 34, 479–495.

Karl, D., Bossard, P., 1985. Measurement and significance of ATP and adenine nucleotide pool turnover in microbial cells and environmental samples. J. Microbiol. Methods 3, 125–139.

Kerker, M., Chew, H., Mcnulty, P.J., Kratohvil, J.P., Cooke, D.D., Sculley, M., Lee, M.P., 1979. Light- scattering and fluorescence by small particles having internal structure. J. Histochem. Cytochem. 27, 250–263.

Kerker, M., 1983. Elastic and inelastic light scattering in Flow Cytometry (Paul Mullaney Memorial Lecture). Cytometry 4, 1–7.

Key, T., Mccarthy, A., Campbell, D.A., Six, C., Roy, S., Finkel, Z.V., 2010. Cell size trade-offs govern light exploitation strategies in marine phytoplankton. Environ. Microbiol. 12, 95–104.

Knap, A.H., Michaels, A.F., Dow, R.L., Johnson, R.J., 1997. Bermuda Atlantic Time-series Study, BATS Method Manual—Version 3. US JGOFS Planning and Coordination Office, Woods Hole, MA.

Knauer, G., Martin, J., Bruland, K., 1979. Fluxes of particulate carbon, nitrogen, and phosphorus in the upper water column of the northeast Pacific. Deep–Sea Res. 26, 97–108.

Landry, M., Kirchman, D., 2002. Microbial community structure and variability in the tropical Pacific. Deep–Sea Res. II 49, 2669–2693.

Li, W., Dickie, P., Irwin, B., Wood, A., 1992. Biomass of bacteria, cyanobacteria, prochlorophytes and photosynthetic eukaryotes in the Sargasso Sea. Deep–Sea Res. 39, 501–519.

Lindell, D., Post, A.F., 1995. Ultraphytoplankton succession is triggered by deep winter mixing in the Gulf of Aqaba (Eilat), RedSea. Limnol. Oceanogr. 40, 1130–1141.

Loken, M.R., Sweet, R.G., Henenberg, L.A., 1976. Cell discrimination by multiangle light scattering. J. Histochem. Cytochem. 24, 284–294.

Lomas, M., Swain, A., Shelton, R., Ammerman, J., 2004. Taxonomic variability of phosphorus stress in Sargasso Sea phytoplankton. Limnol. Oceanogr. 49, 2303–2310.

Lomas, M., Steinberg, D., Dickey, T., Carlson, C.A., Nelson, N., Condon, R., Bates, N.R., 2009. Increased ocean carbon export in the Sargasso Sea is countered by its enhanced mesopelagic attenuation. Biogeosci. Discuss. 6, 9547–9582.

Lomas, M., Burke, A., Lomas, D., Bell, D., Shen, C., Dyhrman, S., Ammerman, J., 2010. Sargasso Sea phosphorus biogeochemistry: an important role for dissolved organic phosphorus (DOP). Biogeosciences 7, 695–710.

Lomas, M., Moran, S., 2010. Evidence for aggregation and export of cyanobacteria and nano-eukaryotes from the Sargasso Sea euphotic zone. Biogeosciences 8, 1–14.

López García, P., Rodriguez Valera, F., Pedros Alió, C., Moreira, D., 2001. Unexpected diversity of small eukaryotes in deep-sea Antarctic plankton. Nature 409, 603–607.

Malmstrom, R.R., Coe, A., Kettler, G.C., Martiny, A.C., Frias-Lopez, J., Zinser, E.R., Chisholm, S.W., 2010. Temporal dynamics of *Prochlorococcus* ecotypes in the Atlantic and Pacific oceans. ISME J. 4, 1252–1264.

Mann, E., Ahlgren, N., Moffett, J., 2002. Copper toxicity and cyanobacteria ecology in the Sargasso Sea. Limnol. Oceanogr. 47, 976–988.

Marañón, E., Cermeno, P., Rodríguez, J., Zubkov, M., Harris, R., 2007. Scaling of phytoplankton photosynthesis and cell size in the ocean. Limnol. Oceanogr. 52, 2190–2198.

Marañón, E., 2008. Inter-specific scaling of phytoplankton production and cell size in the field. J. Plankton Res. 30, 157–163.

Margalef, R., 1978. Life-forms of phytoplankton as survival alternatives in an unstable environment. Oceanol. Acta 134, 493–509.

Michaels, A., Knap, A., 1996. Overview of the U.S. JGOFS Bermuda Atlantic Time-series Study and the Hydrostation S program. Deep–Sea Res. II 43, 157–198.

Moore, L.R., 1997. Physiological Ecology of *Prochlorococcus:* A Comparison of Isolates from Diverse Oceanic Regimes. Ph.D. Thesis. Department of Civil and Environmental Engineering. Massachusetts Institute of Technology.

Moore, L.R., Chisholm, S.W., 1999. Photophysiology of the marine cyanobacterium *Prochlorococcus*: ecotypic differences among cultured isolates. Limnol. Oceanogr. 44, 628–638.

Moore, L., Coe, A., Zinser, E., Saito, M., Sullivan, M.B., Lindell, D., Frois-Moniz, K., Waterbury, J., Chisholm, S.W., 2007. Culturing the marine cyanobacterium *Prochlorococcus*. Limnol. Oceanogr. Methods 5, 353–362.

Morel, A., Ahn, Y., Partensky, F., Vaulot, D., Claustre, H., 1993. *Prochlorococcus* and *Synechococcus*: a comparative study of their optical properties in relation to their size and pigmentation. J. Mar. Res. 51, 617–649.

Mullaney, P.F., Dean, P.N., 1969. Cell sizing—A small-angle light-scattering method for sizing particles of low relative refractive index. Appl. Opt. 8, 2361–2362.

Not, F., Gausling, R., Azam, F., Heidelberg, J.F., Worden, A.Z., 2007. Vertical distribution of picoeukaryotic diversity in the Sargasso Sea. Environ. Microbiol. 9, 1233–1252.

Olson, R.J., Zettler, E.R., Altabet, M.A., Chisholm, S.W., 1990. Spatial and temporal distributions of prochlorophyte picoplankton in the North Atlantic Ocean. Deep–Sea Res. 37, 1033–1051.

Parsons, R.J., Breitbart, M., Lomas, M.W., Carlson, C.A., 2011. Ocean time-series reveals recurring seasonal patterns of virioplankton dynamics in the north-western Sargasso Sea. ISME J., http://dx.doi.org/10.1038/ismej.2011.101.

Partensky, F., Hoepffner, N., Li, W., Ulloa, O., Vaulot, D., 1993. Photoacclimation of *Prochlorococcus* sp.(Prochlorophyta) strains isolated from the North Atlantic and the Mediterranean Sea. Plant Physiol. 101, 285–296.

Partensky, F., Hess, W., Vaulot, D., 1999. *Prochlorococcus*, a marine photosynthetic prokaryote of global significance. Microbiol. Mol. Biol. Rev. 63, 106–127.

Petres, J., Dezelic, G., 1975. Light scattering by large ellipsoidal particles. I. Rayleigh–Debye approach. J. Colloid Interface Sci. 50, 296–306.

R-Development Core Team, 2011. R: a language and environment for statistical computing. R Foundation for Statistical Computing, Vienna, Austria. ISBN 3-900051-07-0, URL ⟨http://www.R-project.org/⟩.

Rajwa, B., Venkatapathi, M., Ragheb, K., Banada, P.P., Hirleman, E.D., Lary, T., Robinson, J.P., 2008. Automated classification of bacterial particles in flow by multiangle scatter measurement and support vector machine classifier. Cytometry A73, 369–379.

Rayleigh, L., 1910. The incidence of light upon a transparent sphere of dimensions comparable with the wave-length. Proc. R. Soc. London Ser. A 84, 25–46.

Robertson, B., Button, D., Koch, A., 1998. Determination of the biomasses of small bacteria at low concentrations in a mixture of species with forward light scatter measurements by flow cytometry. Appl. Environ. Microbiol. 64, 3900–3909.

Rocap, G., Larimer, F.W., Lamerdin, J., Malfatti, S., Chain, P., Ahlgren, N.A., Arellano, A., Coleman, M.L., Hauser, L., Hess, W.R., Johnson, Z.I., Land, M., Lindell, D., Post, A.F., Regala, W., Shah, M., Shaw, S.L., Steglich, C., Sullivan, M.B., Ting, C.S., Tolonen, A., Webb, E.A., Zinser, E.R., Chisholm, S.W., 2003. Genome divergence in two *Prochlorococcus* ecotypes reflects oceanic niche differentiation. Nature 424, 1042–1047.

Rodwell, M., Rowell, D., Folland, C., 1999. Oceanic forcing of the wintertime North Atlantic Oscillation and European climate. Nature 398, 320–323.

Salzman, G.C., Crowell, J.M., Goad, C.A., 1975. A flow-system multiangle light-scattering instrument for cell characterization. Clin. Chem. 21, 1297–1304.

Salzman, G.C., Wilder, M.E., Jett, J.H., 1979. Light scattering with stream-in-air flow systems. J. Histochem. Cytochem. 27, 264–267.

Salzman, G.C., Singham, S.B., Johnston, R.G., Bohren, C.F., 1990. Light scattering and cytometry. In: Melamed, M.R., Lindmo, T., Mendelsohn, M.L. (Eds.), Flow Cytometry and Sorting (2 Ed.). Wiley-Liss, New York, pp. 824, xii.

Shalapyonok, A., Olson, R.J., Shalapyonok, L.S., 2001. Arabian Sea phytoplankton during Southwest and Northeast Monsoons 1995: composition, size structure and biomass from individual cell properties measured by flow cytometry. Deep–Sea Res. II. 48, 1231–1261.

Sharpless, T.K., Traganos, F., Darzynkiewin, Z., Melamed, M.R., 1975. Flow cytofluorimetry: discrimination between single cells and cell aggregates by direct size measurements. Acta Cytol. 19, 577–581.

Please cite this article as: Casey, J.R., et al., Changes in partitioning of carbon amongst photosynthetic pico- and nano-plankton groups in the Sargasso Sea in.... Deep-Sea Res. II (2013), http://dx.doi.org/10.1016/j.dsr2.2013.02.002

Sharpless, T.K., Melamed, M.R., 1976. Estimation of cell size from pulse shape in flow cytofluorometry. J. Histochem. Cytochem. 24, 257–261.
Sharpless, T.K., Bartholdi, M., Melamed, M.R., 1977. Size and refractive index dependence of simple forward angle scattering measurements in a flow system using sharply focused illumination. J. Histochem. Cytochem. 25, 845–856.
Shapiro, H.M., 1977. Fluorescent dyes for differential counts by flow cytometry: does histochemistry tell us much more than cell geometry? J. Histochem. Cytochem. 25, 976–989.
Shaw, S.L., 2001. The Production of Non-Methane Hydrocarbons by Marine Plankton. Ph.D. Thesis. Massachusetts Institute of Technology.
Siegel, D., 1987. On the parameterization of irradiance for open ocean photo-processes. J. Geophys. Res. 92, 14648–14662.
Siegel, D.A., Iturriaga, R., Bidigare, R.R., Smith, R.C., Pak, H., Dickey, T.D., Marra, J., Baker, K.S., 1990. Meridional variations of the springtime phytoplankton community in the Sargasso Sea. J. Mar. Res. 48, 379–412.
Sloot, P., Hoekstra, A., van der Liet, H., Figdor, C., 1989. Scattering matrix elements of biological particles measured in a flow through system: theory and practice. Appl. Opt. 28, 1752–1762.
Sode, K., Oonari, R., Oozeki, M., 1997. Induction of a temperate marine cyanophage by heavy metal. J. Mar. Biotechnol. 5, 178–180.
Sprintall, J., Tomczak, M., 1992. Evidence of the barrier layer in the surface layer of the tropics. J. Geophys. Res. 97, 7305–7316.
Steinberg, D., Carlson, C.A., Bates, N.R., Johnson, R., Michaels, A., Knap, A., 2001. Overview of the US JGOFS Bermuda Atlantic Time-series Study (BATS): a decade-scale look at ocean biology and biogeochemistry. Deep–Sea Res. II 48, 1405–1447.
Talley, L., Raymer, M.E., 1982. Eighteen degree water variability. J. Mar. Res. 40, 757–775.
Ting, C., Rocap, G., King, J., Chisholm, S.W., 2002. Cyanobacterial photosynthesis in the oceans: the origins and significance of divergent light-harvesting strategies. TRENDS Microbiol. 10, 134–142.
Torres-Valdes, S., Rousseau, V., Sanders, R.W., Reynolds, S., Pan, X., Mather, R., Landolfi, A., Wolff, G., Achterberg, E., Williams, R., 2009. Distribution of dissolved organic nutrients and their effect on export production over the Atlantic Ocean. Global Biogeochem. Cycles 23, GB4019, doi:4010.1029/2008GB003389.
Ulicny, J., 1992. Lorenz-Mie light scattering in cellular biology. Gen. Physiol. Biophys. 11, 133–151.
Van Heukelem, L., Thomas, C., 2001. Computer-assisted high-performance liquid chromatography method development with applications to the isolation and analysis of phytoplankton pigments. J. Chromatogr. 910, 31–49.
Veldhuis, M., Kraay, G., Van Bleijswijk, J., Baars, M., 1997. Seasonal and spatial variability in phytoplankton biomass, productivity and growth in the north-western Indian Ocean: the southwest and northeast monsoon, 1992–1993. Deep Sea Res. Part I 44, 425–449.
Veldhuis, M., Kraay, G., 2004. Phytoplankton in the subtropical Atlantic Ocean: towards a better assessment of biomass and composition. Deep–Sea Res. Part I 51, 507–530.
Visbeck, M., Hurrell, J., Polvani, L., Cullen, H., 2001. The North Atlantic Oscillation: past, present, and future. Proc. Natl. Acad. Sci. USA. 98, 12876.
Wang, W., Anderson, B., Kaufmann, R., Myneni, R., 2004. The relation between the North Atlantic Oscillation and SSTs in the North Atlantic basin. J. Clim. 17, 4752–4759.
Woods, J.D., Barkman, W., 1986. A lagrangian mixed layer model of Atlantic 18 °C water formation. Nature 319, 574–576.
Worden, A., Nolan, J., Palenik, B., 2004. Assessing the dynamics and ecology of marine picophytoplankton: the importance of the eukaryotic component. Limnol. Oceanogr. 49, 168–179.
Worden, A., Allen, A.E., 2010. The voyage of the microbial eukaryote. Curr. Opin. Microbiol. 13, 652–660.
Worthington, L.V., 1976. On the North Atlantic Circulation. The Johns Hopkins Oceanographic Studies 6, 110.
Zhao, Y., Ma, L., 2009. Applicable range of the Rayleigh–Debye–Gans theory for calculating the scattering matrix of soot aggregates. Appl. Opt. 48, 591–597.
Zubkov, M., Sleigh, M., Burkill, P.H., Leakey, R., 2000. Picoplankton community structure on the Atlantic Meridional Transect: a comparison between seasons. Prog. Oceanogr. 45, 369–386.
Zwirglmaier, K., Jardillier, L., Ostrowski, M., Mazard, S., Garczarek, L., Vaulot, D., Not, F., Massana, R., Ulloa, O., Scanlan, D.J., 2007. Global phylogeography of marine Synechococcus and *Prochlorococcus* reveals a distinct partitioning of lineages among oceanic biomes. Environ. Microbiol. 10, 147–161.

Please cite this article as: Casey, J.R., et al., Changes in partitioning of carbon amongst photosynthetic pico- and nano-plankton groups in the Sargasso Sea in.... Deep-Sea Res. II (2013), http://dx.doi.org/10.1016/j.dsr2.2013.02.002